A Strategy to Construct Multifunctional Ammonium Polyphosphate for Epoxy Resin with Simultaneously High Fire Safety and Mechanical Properties

Zhu-Bao Shao[a,b], *Jing Zhang*[b], *Rong-Kun Jian*[b,d*], *Chang-Chun Sun*[b], *Xiao-Lu Li*[b], *De-Yi Wang*[b,c*]

[a]Institute of Functional Textiles and Advanced Materials, College of Textiles and Clothing, National Engineering Research Center for Advanced Fire-Safety Materials D & A (Shandong), State Key Laboratory of Bio-Fibers and Eco-Textiles Qingdao University, Ningxia Road, 308, Qingdao 266071, China

[b]IMDEA Materials Institute, C/Eric Kandel, 2, Getafe, Madrid, 28906, Spain

[c]Universidad Francisco de Vitoria, Ctra. Pozuelo-Majadahonda Km 1,800, 28223, Pozuelo de Alarcón, Madrid, Spain

[d]Fujian Provincial Key Laboratory of Polymer Materials, College of Chemistry and Materials Science, Fujian Normal University, Fuzhou 350007, China

Corresponding authors:

*Rong-Kun Jian, Email: jrkht1987@fjnu.edu.cn;

*De-Yi Wang, Email: deyi.wang@imdea.org.

Abstract: Obtaining a well balance between the high fire safety and mechanical performance of epoxy resins (EP) is still a challenge for the traditionally intumescent flame retardant. Herein, a new strategy was constructed to realize the highly uniform dispersion of zeolitic imidazolate framework-67 (ZIF-67) on the ammonium polyphosphate (APP) through the coordination reaction of the pre-bonded Co^{2+} cations with phosphate and 2-methyimidazole. The as-obtained ZIF-67@APP in the loading of 5 wt% endowed EP with a LOI value of 28.5% and UL-94 V0. Furthermore, peak of heat release rate (PHRR) and smoke production rate (SPR) of ZIF-67@APP/EP were greatly decreased by 67.4% and 46.2% compared to EP with 5 wt% APP. The improved fire safety of ZIF-67@APP/EP was ascribed to the faster formation of the expanded char owing to the catalysis of cobalt cation. Meanwhile, the good compatibility between ZIF-67@APP and EP also presented better mechanical properties.

Keywords: epoxy resin; smoke suppression; fire safety; mechanical properties

1. Introduction

Ammonium polyphosphate had been extensively applied to enhance the fire safety of polymer materials owing to its high phosphorus and nitrogen contents [1-2]. It could contribute together with some char agents or easy char-formed groups to form intumescent char layer which could protect the underlying polymer materials from the transfer of heat and oxygen when polymer materials suffered from the fire [3-4]. Particularly, APP could be used alone as flame retardant for EP due to the abundant existence of -OH and benzene- in the EP chains [5-6]. However, to fulfill the satisfactory flame retardance of EP, high loading level of APP was needed because the formation rate and quality of char layer were low after ignition. What's worse, excessive addition of APP usually induced the mechanical deterioration of EP, which limited the further application of APP [7]. Therefore, how to obtain the high flame-retardant efficiency of APP attracted the researchers' attention.

Now, the introductions of some char agents or easy char-formed groups on the surface of APP or blending with APP to form the satisfactory char layer were the common strategy. In Wang's group [8-9], some aliphatic polyamines, such as triethylene tetramine, piperazine and polyethylenimine had been employed on modification of APP, and the results exhibited that the char layer of cured EP was improved and some mechanical performance also enhanced. Subsequently, large decrease of PHRR indicated the enhancement on fire safety. Polyphosphazenes-encapsulated APP (PZMA@APP) had been prepared and used to flame retard EP, which could pass the UL-94 V0 rating with the loading of 10 wt% PZMA@APP [10]. Unfortunately, these loadings of modified APPs were still high and the problem about mechanical deterioration was not solved. Thus, novel strategy to modify APP should be considered about the fire safety for EP.

More recently, researchers had focused on the synergistic effect between APP and metal elements for polymer materials due to some metal elements could accelerate the phosphorylation of hydroxyl group, indicated that more phosphorylation cross-linking structures were generated, which could diminish the heat flow exposed on the surface of the materials and improve the barrier effect of char layers [11-13]. A series of mixture of APP and metal salts or oxides, such as cuprous oxide, cobalt acetate (CoAc), manganese acetate (MnAc), nickel acetate (NiAc) and zinc acetate (ZnAc) etc. were utilized to reduce the fire hazard of polymer materials [14-18]. The results showed that these flame retardants not only decreased the heat release but also diminished the smoke product through enhancement on the formation of the char layers. Nonetheless, the low dispersity and mechanical deterioration of APP and metal salts for polymer materials were not idea to fulfil the further application.

Metal organic frameworks (MOFs) consisted of metal ions and organic ligands had developed fast in catalysis, gas storage and sensor etc [19-20] due to its advantages on permanent pore structure, large surface area, and adjustable pore size [21-22], which endowed the MOFs with combination of thermal barrier effect and high-efficient catalysis [23]. Meanwhile, the various organic groups could bring some special properties, such as improvement on compatibility between polymer and MOF$_S$ [24]. Especially, in the recent work, the ability of MOFs on the rapid catalytic formation of char layer and enhancement on mechanical performance for EP had been found when it suffered from the fire [25-27]. However, the fire safety of MOFs/EP composites could not fulfil the requirement of application due to the char lay could not remain during combustion [28]. Therefore, much work had focused on the synergistic effect between APP and MOFs [29]. For example, the synergistic effect between APP and MOF@GO on EP was discussed and the better charring catalysis ability was revealed, and the stable char layer could be

formed at low temperature about 400 °C [30]. ZIF-67, the coordination polymer of 2-methylimidazole and cobalt, as one of the widely used MOFs was also used in flame-retarding polymers. Hao's group [31] had directly chemically modified APP by ZIF-67 particles for flame retarding ethylene-vinyl acetate, and the results displayed synergistic effect between APP and ZIF-67. However, only a few of ZIF-67 particles were deposited on the surface of APP and the dispersion of ZIF-67 was uneven due to the weak reaction ability between APP and ZIF-67 particles. Therefore, a new strategy for the modification of APP by MOFs needed to be built.

In this work, we found a tactful route to synthesize chemically surface-assembled APP (ZIF-67@APP) by ZIF-67. Herein, firstly, the ion exchange reaction was designed and carried out between APP and cobalt (II) nitrate hexahydrate at certain condition to produce the active reaction points (Co (II)) on the surface of APP (Co@APP), which could act as an ideal template to fix the location of the ZIF-67. Then the ZIF-67 could grow on the surface of APP according to these active reaction points with 2-methylimidazole. Various characterizations were employed on confirming the chemical composition and micro-morphology of ZIF-67@APP. Meanwhile, the mechanical properties and fire safety of ZIF-67@APP/EPs were illustrated using adequate measurements. In addition, the possible mechanism of enhancement on the compatibility and reduce on the fire hazard of ZIF-67@APP/EPs comparing with APP/EP were further evaluated.

2. Experimental Section

2.1 Materials

Ammonium polyphosphate (FR CROS 484, Phase II) was obtained from Budenheim Ibérica S.L.U.; Cobalt (II) nitrate hexahydrate ($Co(NO_3)_2 \cdot 6H_2O$) was supplied by United Kingdom; 2-Methylimidazole (≥98.0%) was purchased from Tokyo chemical industry Co. LTD;

Epoxy resin L20 with epoxy value of 0.56 mol/100 g was supplied by R&G Faserverbundwerkstoffe GmbH (Germany); 4,4´-Diaminodiphenylmethane (DDM, ≥97.0%, GC) was purchased from Sigma-Aldrich Chemical Co. LTD; Ethanol (96.0%) was obtained from Productos DISOPOL, S. A.

2.2 Synthesis of ZIF-67 and ZIF-67@APP

2.2.1 Synthesis of ZIF-67

The ZIF-67 was obtained according to the previous literature [32]. Firstly, 1.45 g (5 mmol) $Co(NO_3)_2 \cdot 6H_2O$ and 8.20 g (100 mmol) 2-methylimidazole were dissolved in 150 mL and 50 mL ethanol through ultrasonic dispersion under room temperature, respectively. Then the $Co(NO_3)_2 \cdot 6H_2O$ solution and 2-methylimidazole solution was mixed slowly, and the mixture solution remained stirring at room temperature for 12 h. After that, the mixture was obtained by centrifugation and washed with ethanol five times. Finally, the resulted product was dried in oven for 12 h at 90 °C.

2.2.2 Surface-assembly of ZIF-67 (ZIF-67@APP)

4 g APP was first added into a 500 mL flask, and then 1.45 g (5 mmol) $Co(NO_3)_2 \cdot 6H_2O$ dissolved in 150 mL ethanol was poured into the flask with stirring at room temperature for 2 h. Afterwards, 8.20 g (20 mmol) 2-methylimidazole dissolved in 50 mL ethanol was added into the flask slowly, and the reaction mixture kept stirring at room temperature for 12 h. The purple solid was obtained through centrifugation and further purified by washing with ethanol five times. Finally, the resulted product was dried in oven for 12 h at 80 °C. The modified loading of ZIF-67 on the surface of ZIF-67@APP yielded 8.8 wt%. The detailed preparation process of ZIF-67@APP was shown as Scheme 1.

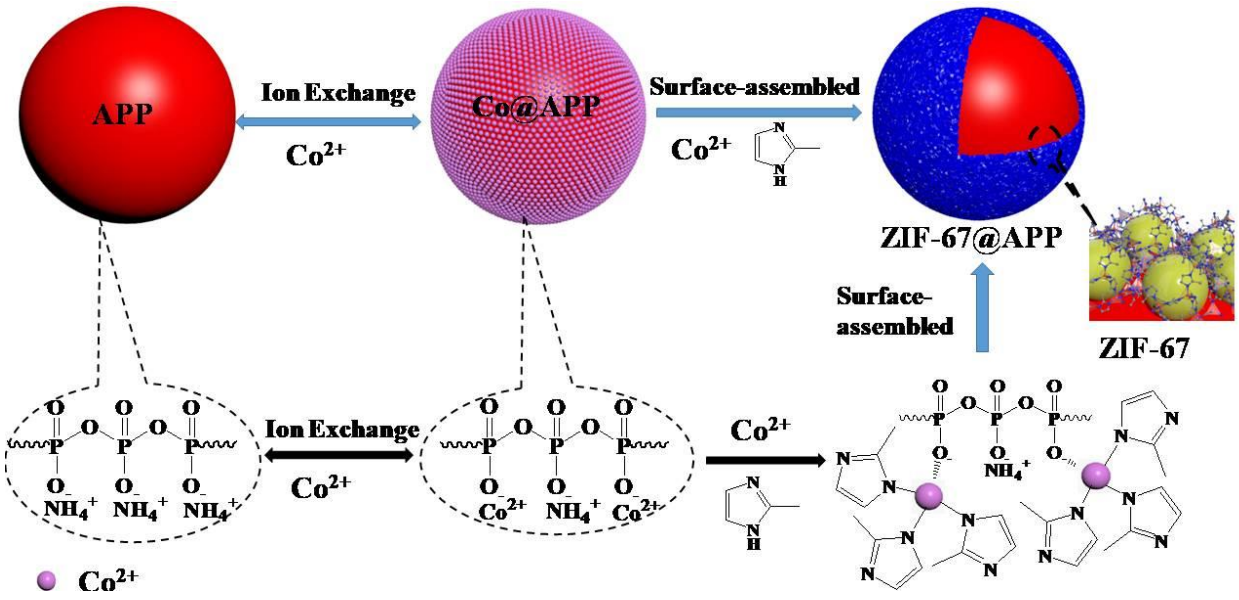

Scheme 1. The synthetic route of ZIF-67@APP

2.3 Fabrication of ZIF-67@APP/EPs and corresponding EPs

The formulations of the pure EP, APP/EP, (ZIF-67+APP)/EP and ZIF-67@APP/EPs were displayed in Table 1, and the preparation route was as follows. Typically, ZIF-67@APP were mixed with EP under magnetically stirring, then the mixture kept stirring at 90 °C for 0.5 h, followed by ultrasonic dispersion for 10 min. Thereafter, DDM was added to the mixture and remained stirring at 90 °C for another 20 min. Finally, the mixture was poured into a pre-heated mold and cured at 100 °C for 2 h and 150 °C for 2 h. In addition, the pure EP, APP/EP and (ZIF-67+APP)/EP were prepared through the same process.

Table 1. Formulations of ZIF-67@APP/EPs and corresponding EPs

Samples	EP (g)	DDM (g)	APP (g)	ZIF-67 (g)	ZIF-67@APP (g)
Pure EP	50.0	14.1	-	-	-

5APP/EP	50.0	14.1	3.4	-	-
5(ZIF-67+APP)/EP	50.0	14.1	3.1	0.3	-
1ZIF-67@APP/EP	50.0	14.1	-	-	0.65
3ZIF-67@APP/EP	50.0	14.1	-	-	2.0
5ZIF-67@APP/EP	50.0	14.1	-	-	3.4

2.4 Characterization

XRD data of samples were recorded by a diffractometer (Empyrean, PANalytical) with Cu Kα radiation (λ=0.154) under the 2θ range from 5 to 70°; The morphological features of samples were investigated by scanning electron microscope (SEM, EVO MA15, Zeiss) equipped with energy dispersive X-ray spectroscopy (EDS). The particle sizes of samples were tested by Bettersizer laser particle size analyzer (Dandong, China); Cobalt content of ZIF-67@APP was tested by inductively coupled plasma-atomic emission spectrometry (ICP-AES, USA); X-ray photoelectron spectroscopy tests were carried out by ESCALAB 250Xi (USA) with Al Ka excitation radiation (hν=1486.6 eV).

Tensile and Flexural properties were carried out the INSTRON-3384 testing machine (UK) according to standard ASTM D638 and ASTM D790 with a speed of 2 mm/min, respectively.

The thermomechanical properties were recorded by dynamic mechanical analyzer (DMA Q 800, TA, America). The specimens were used with single cantilever model under the constant frequency of 1.0 Hz, the oscillation amplitude was 10.0 μm, and the heating rate was 3 °C/min.

Differential scanning calorimetry (DSC) were tested by a TA Q200 analyzer at the heating rate of 5 ℃/min from 0 ℃ to 280 ℃ with nitrogen atmosphere. For DSC tests, the samples, such as

5APP+EP and 5ZIF-67@APP+EP were prepared as follows: APP and ZIF-67@APP were mixed with EP and kept stirring at 90 °C for 0.5 h, respectively. After that, ultrasonic dispersion was used for 10 min, then cooled down to room temperature. As for EP+DDM, 5APP+EP+DDM and 5ZIF-67@APP+EP+DDM, the early prepared process was same to that before ultrasonic dispersion, after that, DDM was added to the mixture and remained stirring at 90 °C for 20 min, finally, cooled down to room temperature.

Thermogravimetric (TG) tests were displayed on thermal gravimetric analyzer (TA Q50) using the nitrogen atmosphere, and the heating temperature range from 40 °C to 700 °C under the heating rate of 10 °C/min.

The limiting oxygen index (LOI) values were collected by LOI instrument (FTT, UK) according to ASTM D 2863-2013 with the size of the samples was 120 × 6.5 × 3.2 mm^3; Vertical burning level tests of samples were measured by FTT instrument (UK) according to ASTM D 3801 with the size of samples was 120 × 13 × 3.2 mm^3; Combustion behaviors of the samples were employed on a cone calorimeter device (CC, Fire Testing Technology, UK) with the samples size of 100 × 100 × 3 mm^3 under a heat flux of 50 kW/m^2.

Laser Raman spectroscopy data were collected by a SPEX-1403 laser Raman spectrometer with 514.5 nm argon laser. (SPEX Co., USA). Two absorption peaks at about 1580 cm^{-1} and 1360 cm^{-1} were ascribed to the G band and the D band, respectively. And I_D/I_G ratios of samples were calculated from the intensity ratios fitted D and G bands.

Fourier transform infrared spectroscopy (FTIR) was performed on Nicolet 170SX spectrometer over the wavenumber of 500-4000 cm^{-1}.

Thermo-Raman spectrum was obtained by RM 2000 laser Raman spectrometer with 514.5 nm argon laser (Renishaw, UK), and the heating temperature range from 450 °C to 710 °C under the heating rate of 10 °C/min.

3. Results and Discussion

3.1 Characterization of ZIF-67@APP

The crystal structures of APP, ZIF-67 and ZIF-67@APP were characterized by XRD and corresponding patterns were displayed as Figure 1. The characterized peaks about ZIF-67 were in agreement with the theoretical data according to the literatures [32-33], indicating that the ZIF-67 was successfully prepared and excellent crystallinity was achieved. Through comparison with the XRD patterns of APP and ZIF-67, it could be found both the diffraction peaks of APP and ZIF-67 were overall exhibited on the XRD patterns of ZIF-67@APP and no other new peaks appeared, suggesting this modified reaction was feasible to prepare ZIF-67@APP.

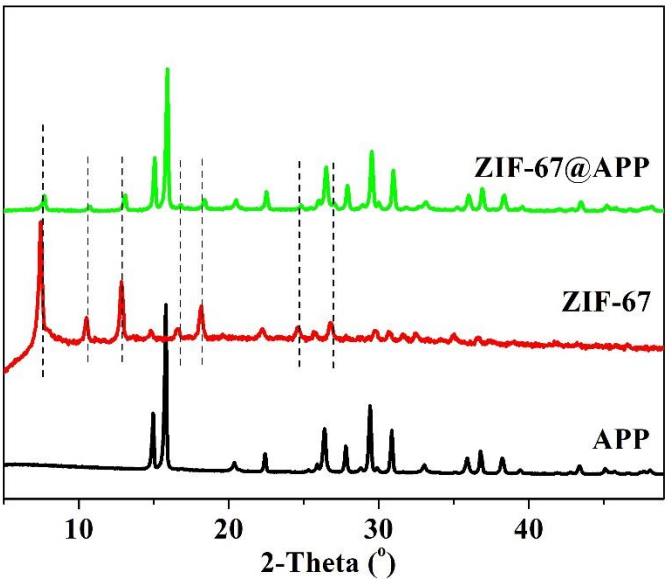

Figure 1. XRD patterns of APP, ZIF-67, and ZIF-67@APP.

The particle size analyzer was further utilized to investigate the particle size of ZIF-67@APP, and the detailed data was shown as Figure S1. Herein, the excellent particle size distribution of

APP was displayed with an average particle size of 16.96 μm. After modification by ZIF-67, the average particle size of ZIF-67@APP increased to 18.15 μm. Meanwhile, compared with APP, the shape of the particle size distribution of ZIF-67@APP was sharper and there were less ZIF-67@APP below the particle size of 2 μm, indicating that ZIF-67@APP owned better particle size distribution than that of APP.

The surface morphologies of APP and ZIF-67@APP particles were characterized by SEM as Figure 2. It could be clearly observed that unmodified APP particles displayed smooth surface. Meanwhile, the particle sizes of ZIF-67 ranged from 100 nm-500 nm. Comparing to APP, ZIF-67@APP presented a rough surface, which was caused by the dispersion of ZIF-67 particles on the surface of APP. As seen in Figure 2c´, ZIF-67 was anchored uniformly on the surface of APP without massive accumulation. Besides, the EDS test was also utilized to analyze the element distribution on the surface of ZIF-67@APP in Figure 3, the appearance of Co and C element on the surface of ZIF-67@APP further demonstrated that ZIF-67@APP was obtained.

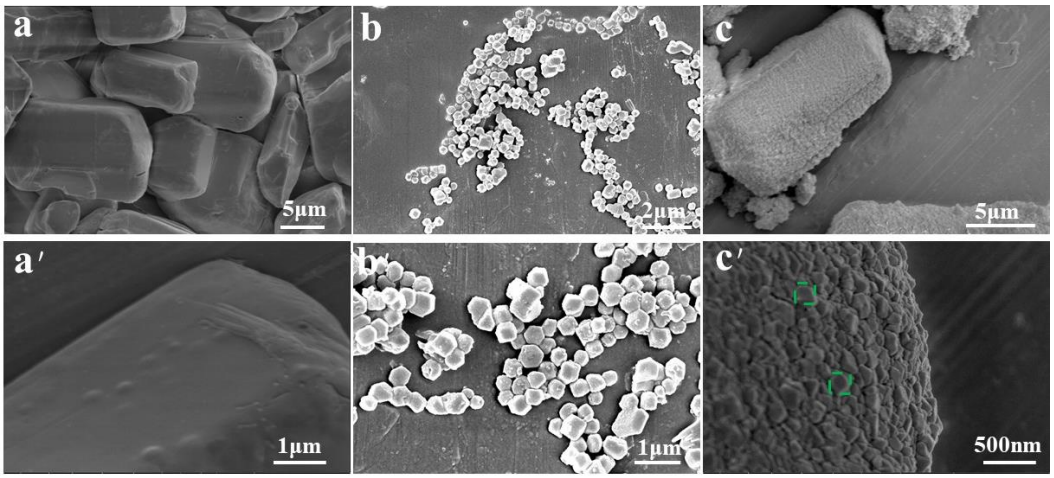

Figure 2. The morphology of pure APP (a, a´), ZIF-67(b, b´) and ZIF-67@APP (c, c´).

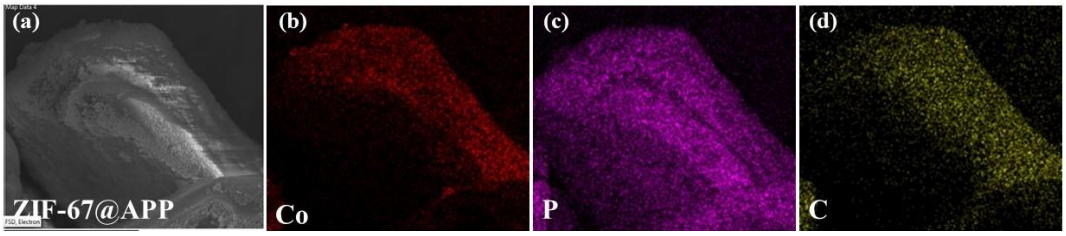

Figure 3. The corresponding morphology of ZIF-67@APP (a) and elements mapping of Co (b), P (c), and C (d).

The O_{1s} spectra of APP and ZIF-67@APP were displayed as Figure 4. Herein, two peaks of APP at binding energy of 531.1 eV and 533.0 eV were ascribed to the P=O, -O- and $-O^{-}$ NH_4^{+} [34-35], respectively. For ZIF-67@APP, except for above two peaks, a new band was observed at 531.7 eV, which could be assigned to $-O^{-}$ Co^{2+} between ZIF-67 and APP. By virtue of the presence of $-O^{-}$ Co^{2+}, it suggested that ZIF-67 was chemically bonded with APP, and in this case, ZIF-67 gradually grew and was further anchored evenly in the surface of APP. The presence of $-O^{-}$ Co^{2+} further suggested that ZIF-67@APP was prepared successfully.

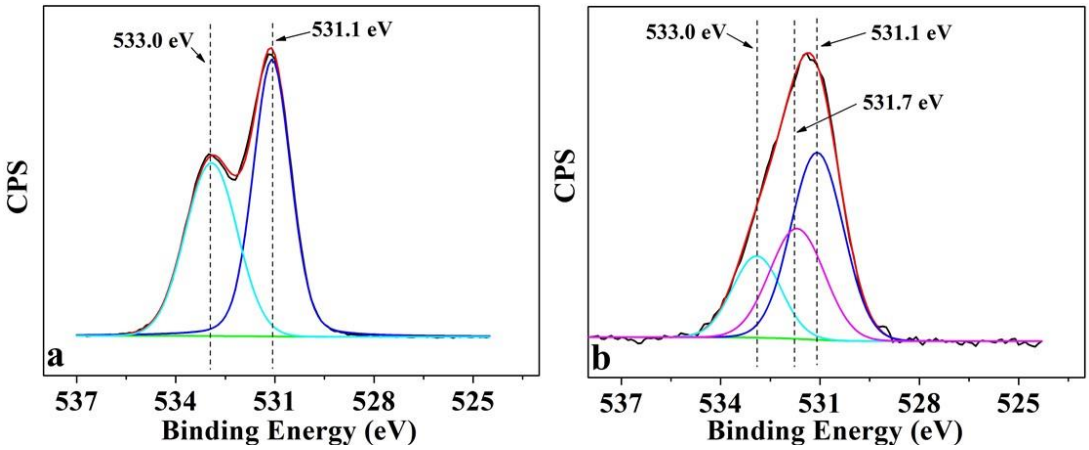

Figure 4. O_{1s} spectra of APP (a) and ZIF-67@APP (b).

3.2 Mechanical behavior of ZIF-67@APP/EPs and corresponding EPs

The mechanical properties of ZIF-67@APP/EPs and corresponding EPs were illustrated by the tensile strength, flexural strength and strain-to-failure, and the relevant results were listed in Table 2. By comparison with 5APP/EP, the tensile strength, flexural strength and strain-to-failure of 5ZIF-67@APP/EP were improved from 53.6 MPa, 55.3 MPa and 5.5% to 63.8 MPa, 79.2 MPa and 7.1%, respectively, indicating that ZIF-67@APP could improve the mechanical performance of EP compared with APP at the same loading. Meanwhile, the tensile strength, flexural strength, and strain-to-failure of 5(ZIF-67+APP)/EP were up to 55.7 MPa, 70.7 MPa and 6.2%, respectively, which were better than those of 5APP/EP, while lower than those of 5ZIF-67@APP/EP. It could be explained by the better compatibility of ZIF-67@APP than APP in the epoxy matrix. To further make the above phenomenon clear, the SEM photos were used to observe the fractured morphologies of APP/EP, ZIF-67@APP/EP and (ZIF-67+APP)/EP in Figure 5. For APP/EP, APP dispersed unevenly in the epoxy matrix, and an obvious “defect” marked in the black arrow appeared between EP and APP particles, indicating the poor interfacial compatibility of them. However, after incorporation of ZIF-67@APP, no gap existed in the interface between ZIF-67@APP and the epoxy matrix, that was to say, the interfacial action between ZIF-67@APP particles and EP was enhanced. As for (ZIF-67+APP)/EP, it could be clearly observed that ZIF-67 marked in white circle and APP distributed dispersedly in the epoxy matrix. What’s more, the gap was found in the interface of APP particles and the epoxy matrix, while not for ZIF-67. It was deduced that the existence of ZIF-67 should be the key to the improved mechanical properties of ZIF-67@APP/EP compared to APP/EP. On one hand, the anchoring of ZIF-67 could increase the specific surface area of APP, as a result, the interaction zone between ZIF-67@APP and the matrix was enlarged. In addition, organic 2-methylimidazole group in the structure of ZIF-67, with a catalytic activity of curing epoxy resins [36], also played

a positive role in improving the interfacial action between ZIF-67@APP and EP. According to the results above, it could be concluded that good interfacial compatibility between ZIF-67@APP and EP resulted from the chemical modification of ZIF-67 on the APP surface.

Table 2. Mechanical properties of the ZIF-67@APP/EPs and corresponding EPs

Sample	Tensile strength (MPa)	Flexural strength (MPa)	Strain-to-failure (%)
Pure EP	73.4±3.6	104.1±4.0	10.0±2.1
5APP/EP	53.6±3.0	66.3±2.7	5.5±0.31
1ZIF-67@APP/EP	78.2±4.0	108.5±3.6	9.1±0.22
3ZIF-67@APP/EP	70.3±3.3	88.4±3.0	8.5±0.30
5ZIF-67@APP/EP	63.8±3.8	79.2±2.9	7.1±0.20
5(ZIF-67+APP)/EP	55.7±2.5	70.7±1.9	6.2±0.25

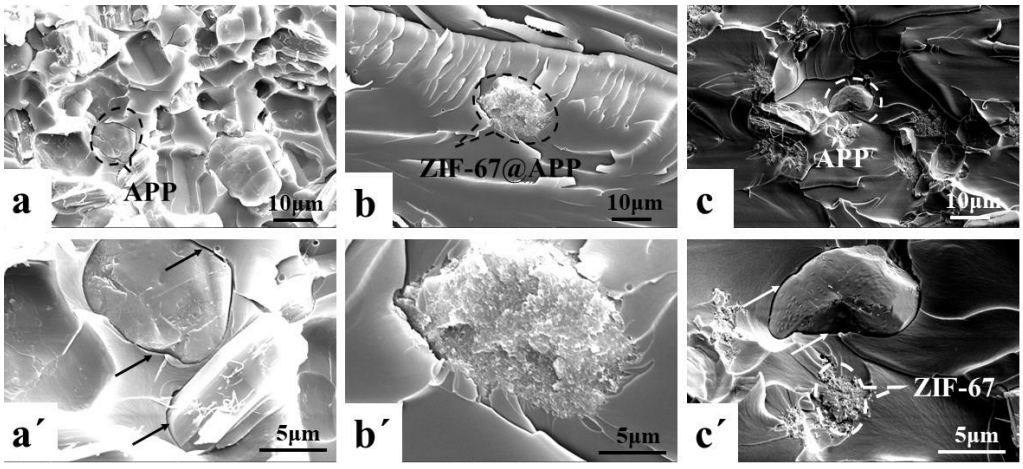

Figure 5. The fractured morphology of APP/EP (a, a´), 5ZIF-67@APP/EP (b, b´) and 5(ZIF-67+APP)/EP (c, c´).

DSC test was employed to illustrate the curing process of epoxy resins in the presence of fillers, and the corresponding results were exhibited on the Figure 6. Herein, for 5APP+EP, no exothermic peak appeared below 250 °C, indicated that the curing process of EP was not affected by APP alone. After the introduction of ZIF-67@APP to EP, an obvious peak appeared between 175 °C and 270 °C, suggesting that ZIF-67@APP could promote the curing process of EP due to the latent curing activity of 2-methylimidazole group. Furthermore, compared with DSC curves of EP+DDM and 5APP+EP+DDM, the peak of 5ZIF-67@APP+EP+DDM shifted from 166 °C to 163 °C. Accordingly, the results revealed that ZIF-67@APP was served as potentially reactive filler and could accelerate the curing process of EP [37-38]. Therefore, ZIF-67@APP could improve the compatibility and mechanical performance of EP comparing with APP.

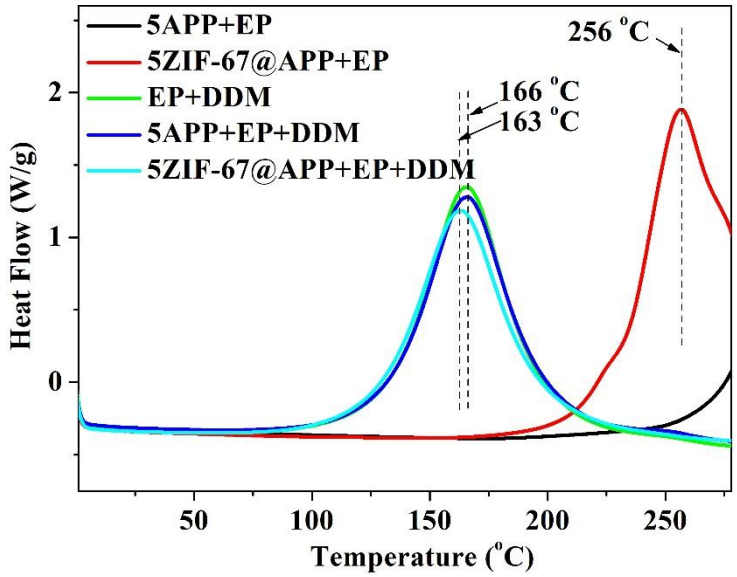

Figure 6. DSC curves of 5APP+EP, 5ZIF-67@APP+EP, EP+DDM, 5APP+EP+DDM and 5ZIF-67@APP+EP+DDM.

3.3 Thermal decomposition and stability behavior of ZIF-67@APP/EPs and corresponding EPs

TGA tests could assist in analyzing the thermal decomposition performances of cured APP/EP and ZIF-67@APP/EPs, and the results were showed in Figure 7, Fig S3 and Table 3. For Figure 7, Pure EP, APP/EP and ZIF-67@APP/EPs all owned one weight-loss decomposition stages from 250 °C to 500 °C. Comparing with pure EP, the initial thermal decomposition of 5APP/EP started early, meanwhile, the maximum weight loss rate of decreased from -1.44 %/min to -1.14%/min and yielded the residue of 20.6 wt% at 700 °C. After incorporation of ZIF-67@APP into the EP, the initial decomposition temperature of the ZIF-67@APP/EP decreased and the maximum weight loss rate decreased with the loading of ZIF-67@APP. When the loading of ZIF-67@APP increased to 5 wt%, the $T_{5\%}$ of ZIF-67@APP/EP reduced to 327 °C, which was lower than that of pure EP and 5APP/EP. Interestingly, 5ZIF-67@APP/EP exhibited the lowest maximum weight loss rate of -0.82 %/min and the most residue of 27.1 wt% among the testing materials. In addition, it was seen that ZIF-67@APP could promote the early degradation compared to pure EP and APP/EP under O_2 atmosphere (Fig S3), and more residue left during 400-600 °C. According to the analyses above, it could be concluded that the introduction of ZIF-67@APP could improve the stability of char layer of EP at high temperature, which were benefit to enhance the flame retardancy of EP.

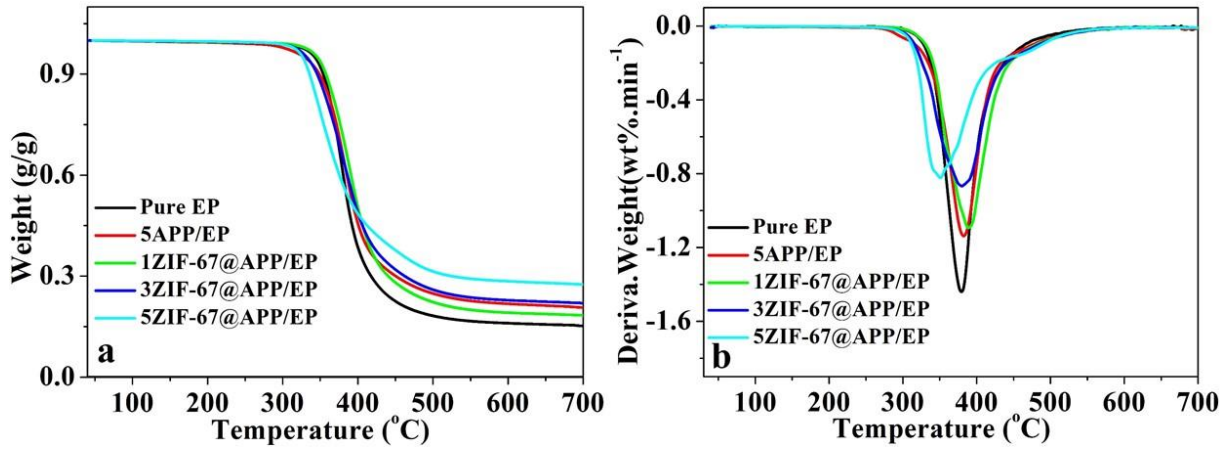

Figure 7. TG (a) and DTG (b) curves of APP/EP and ZIF-67@APP/EPs under N_2 atmosphere.

Table 3. Thermogravimetric data of APP/EP and ZIF-67@APP/EPs under N_2 atmosphere

Samples	$T_{5\%}$[a](°C)	R_{max}[b](%/min)	W_{700}[c] (wt%)
Pure EP	343	-1.44	15.2
5APP/EP	329	-1.14	20.6
1ZIF-67@APP/EP	340	-1.09	18.4
3ZIF-67@APP/EP	332	-0.87	22.0
5ZIF-67@APP/EP	327	-0.82	27.1

[a]The temperature where 5 wt% of weight was lost.

[b]The maximum weight loss rate.

[c]The residual weight at 700 °C.

3.4 Flame-retardant behavior of ZIF-67@APP/EPs and corresponding EPs

LOI and UL-94 tests were the classical methods to evaluate the flame retardancy of polymer materials [39-40]. As shown in Table 4, pure EP failed to pass the UL-94 test, and presented the LOI value of 25.7%. When APP was used to flame retard EP, the LOI value of 5APP/EP

increased to 26.7%, and still could not pass the UL-94 test. For ZIF-67@APP/EP, the LOI values increased with the loading of ZIF-67@APP increase. When the loading of ZIF-67@APP was up to 3 wt%, the LOI value of EP reached 28.3%. Further increasing the content of ZIF-67@APP to 5 wt%, ZIF-67@APP/EP could achieve a higher LOI value as 28.5%, and get a UL-94 V-0 rating. Interestingly, char layers formed fast and little fire could be observed after ignition during the UL-94 test of ZIF-67@APP/EP. The phenomenon was different from that of pure EP and 5APP/EP, suggesting ZIF-67@APP could restrict the release of heat from EP during combustion. Therefore, ZIF-67@APP/EP displayed better flame-retardancy compared with APP/EP and (ZIF-67+APP)/EP. In addition, to the best of our knowledge, epoxy thermosets containing APP or modified APP reported in other literatures always need higher amount of APP or modified APP to achieve the equal results as shown in Table S2, indicating the higher flame-retardant efficiency of ZIF-67@APP.

Table 4. LOI and UL-94 results of ZIF-67@APP/EPs and corresponding EPs

Sample	LOI (%)	UL-94 (3.2 mm)	
		Rating	Time (t_1+t_2, s)
Pure EP	25.7	NR	>50
5APP/EP	26.7	NR	>50
5(ZIF-67+APP)/EP	28.4	V1	14-30
1ZIF-67@APP/EP	26.7	NR	>50
3ZIF-67@APP/EP	28.3	V1	15-30

5ZIF-67@APP/EP	28.5	V0	4-8

The CC test was further introduced to assess the fire-retardant performance of the cured EPs, and the reference samples of pure EP, 5APP/EP, 5(ZIF-67+APP)/EP and ZIF-67@APP/EPs were selected. The corresponding curves and data were collected in Figure 8 and Table 5. It was observed that the time to ignition (TTI) of pure EP was 56 s. After ignition, it burned quickly and reached the PHRR to 1254 kW/m^2 within 115 s, indicating the easy inflammability and immense fire hazard of EP. For APP/EP, the time to PHRR was delayed to 140 s, longer than that of pure EP. Meanwhile, the PHRR value of APP/EP decreased to 924 kW/m^2. When ZIF-67@APP was incorporated into EP, the fast formation of char layer could be observed after ignition, and then the intensity of flame was weakened during CC test (**Video 1**). Therefore, the shoulder peaks appeared after ignition in Figure 8a and a', and the time to PHRR also increased largely, furthermore, the HRR value increased slower than that of APP/EP and pure EP. Besides, TTI of ZIF-67@APP/EPs decreased, which were attributed to the lower thermal stability of ZIF-67@APP in accordance with results of TGA. These phenomena indicated that ZIF-67@APP could promote EP to degrade early, and then the stable char layer formed quickly at the beginning time. Therefore, the shoulder peaks could be observed in the figure and then the char layer could protect the unburned EP from oxygen and heating, and the mass loss rate reduced lower compared with pure EP and 5APP/EP in the Figure 8c. The detailed data was shown as follow: the PHRR of ZIF-67@APP/EP decreased obviously to 603 kW/m^2 when the loading was only 1 wt%, meanwhile, the time to the PHRR increase to 190 s. Accordingly, the fire growth rate (FGR) of 1ZIF-67@APP/EP reduced from 10.9 kW/m^2·s to 3.2 kW/m^2·s, indicting fire hazard of the EP was obviously reduced [41-42]. Interestingly, the flame retardancy of ZIF-67@APP/EP further improved with the loading of ZIF-67@APP increase. As for

5ZIF-67@APP/EP, only the PHRR increased slowly to 150 kW/m^2 even the time reached 178 s. Finally, the PHRR was reduced to 301 kW/m^2 at 285 s, and displayed a low FGR of 1.1 kW/m^2·s, decreased by 67.4% and 83.3% compared with the corresponding values of the APP/EP, respectively. After complete combustion, THR of 5ZIF-67@APP/EP further decreased to 73 MJ/m^2 from 103 MJ/m^2, suggesting the existence of ZIF-67@APP was more conducive to suppress the heating release than APP. Additionally, by comparison with other epoxy thermosets containing APP or modified APP as shown in Table S2, even the amount of ZIF-67@APP in epoxy thermosets was lower, ZIF-67@APP/EP displayed comparative or much lower peak of heat release rate. Besides, the mass loss rate of 5ZIF-67@APP/EP displayed the lower value than that of (ZIF-67+APP)/EP, and the residue of 5ZIF-67@APP/EP left 25.7 wt% after burn-out. Therefore, the above results indicated that ZIF-67@APP can promote the char formation process, and the excellent combination between APP and ZIF-67 could further improve the flame retardancy of EP.

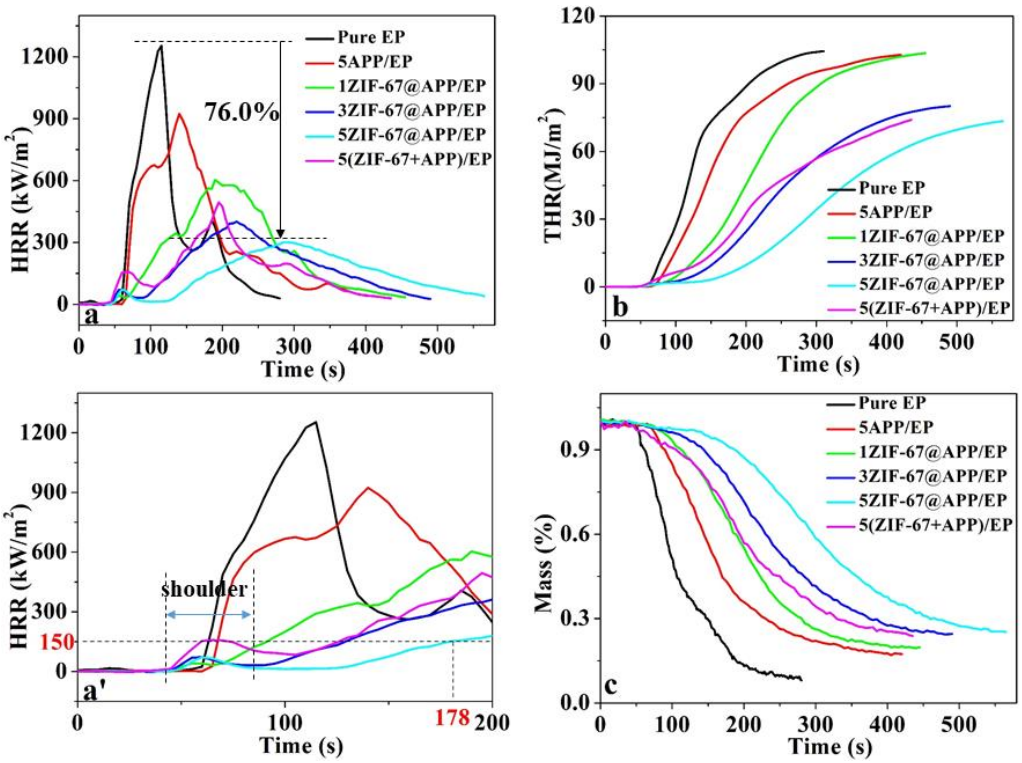

Figure 8. The HRR (a, a´), THR (b), and mass (c) curves of pure EP, 5APP/EP, 1ZIF-67@APP/EP, 3ZIF-67@APP/EP, 5ZIF-67@APP/EP and 5(ZIF-67+APP)/EP.

Generally, most deaths resulted from the smoke during the fire hazard [43-44], hence, SPR, total smoke production (TSP), COP and CO_2 production rate (CO_2P) were the important parameters to evaluate the fire safety of EPs [45]. Here, the SPR and COP of 5ZIF-67@APP/EP dropped to 0.14 m^2/s, 0.01 g/s, respectively, which decreased by 46.2% and 57.4% compared to APP/EP, implying the ZIF-67@APP/EP presented excellent smoke suppression. More interestingly, for 5ZIF-67@APP/EP, the time to the peak of SPR and CO was also delayed largely compared with other EPs in the Figure 9, indicating more time for people to escape from the fire. Therefore, the results showed that the addition of ZIF-67@APP could do better work on restraining the release of smoke to decrease the fire hazard during burning.

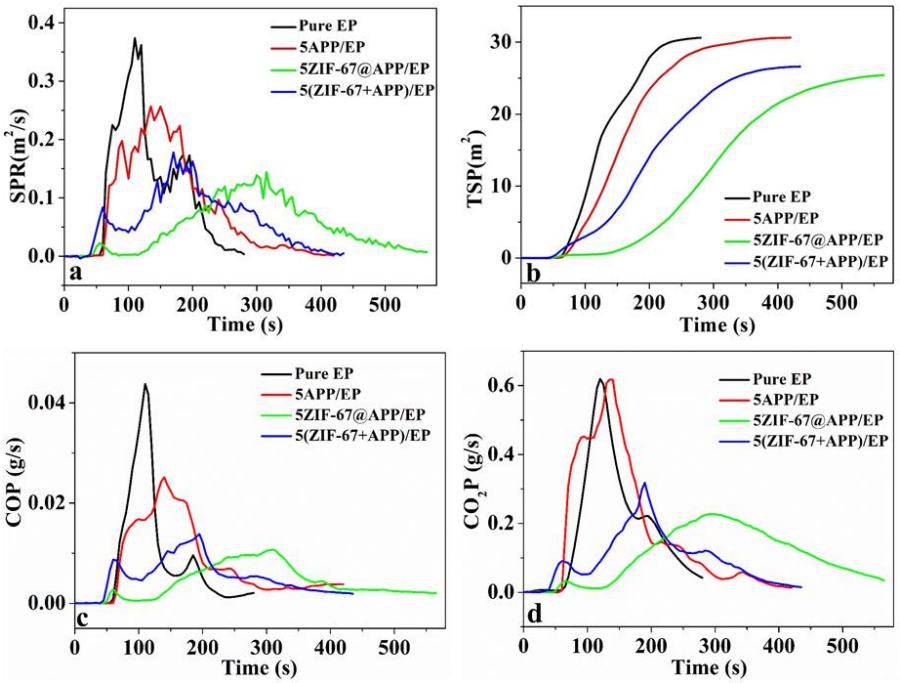

Figure 9. The SPR (a), TSP (b), COP (c), and CO_2P (d) curves of pure EP, 5APP/EP, 5ZIF-67@APP/EP and 5(ZIF-67+APP)/EP.

Table 5. CC data of pure EP, APP/EP, ZIF-67@APP/EPs and (ZIF-67+APP)/EP

Sample	Pure EP	5APP / EP	1ZIF-67 @APP/EP	3ZIF-67 @APP/EP	5ZIF-67 @APP/EP	5(ZIF-67 +APP) /EP
TTI (s)	56	57	47	44	43	41
Peak HRR (kW/m^2)	1254	924	603	401	301	495
Time to PHRR (s)	115	140	190	220	285	195
FGR ($kW/m^2.s$)	10.9	6.6	3.2	1.8	1.1	2.5
THR (MJ/m^2)	105	103	104	80	73	74
Peak SPR (m^2/s)	0.38	0.26	0.17	0.16	0.14	0.16

TSP (m^2)	31	31	31	28	27	27
Residue (%)	8.0	17.4	19.8	24.6	25.7	23.8

The residues of ZIF-67@APP/EPs and corresponding EPs after CC test were exhibited on digital photos in Figure 10. Here, the char residual of pure EP was discontinuous and lots of big holes appeared. When APP or the mixture of APP and ZIF-67 were added to EP, respectively, some holes still existed although the exterior surface of char exhibited intumescent structure. However, for ZIF-67@APP, the exterior surface of char was more intumescent and continuous in comparison to that of APP/EP and pure EP, which could act as an effective barrier between combustion zone and an adjacent unburnt zone and consequently restrained the propagation of flame. [46]

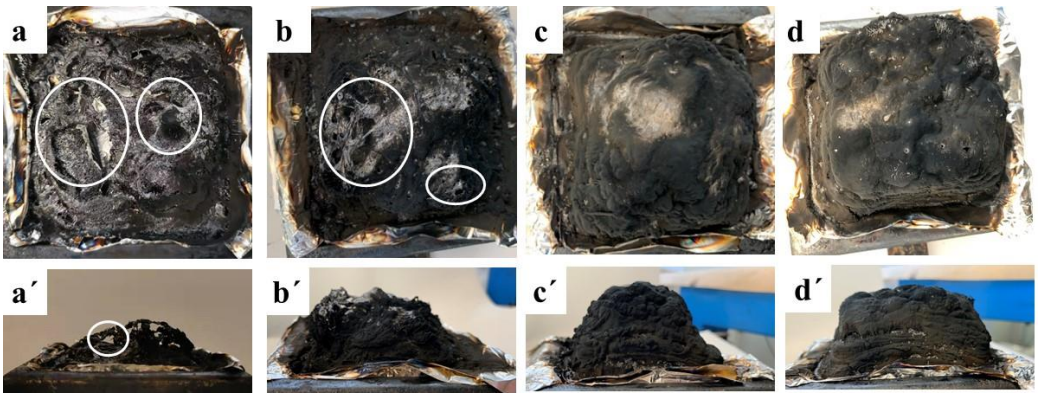

Figure 10. Top view and front view of char residual of pure EP (a, a´), 5APP/EP (b, b´), 5ZIF-67@APP/EP (c, c´) and 5(ZIF-67+APP)/EP (d, d´) after CC test.

Then the SEM images and Raman spectra were utilized to further investigated the charring structure of pure EP, 5APP/EP, 5ZIF-67@APP/EP and 5(ZIF-67+APP)/EP after CC test (Figure 11). Compared with pure EP and APP/EP composite, the (ZIF-67+APP)/EP generated uniform holes on the exterior surface (Figure 11a-d). In terms of ZIF-67@APP/EP, the more compact and

uniform holes appeared on the exterior char layer. For the interior surface, the (ZIF-67+APP)/EP and ZIF-67@APP/EP exhibited integral structure and no holes appeared on the SEM images in comparison to that of pure EP and APP/EP composite (Figure 11a´-d´). In addition, char residual after CC were also carried out illustrating the char structure by the Raman test. The intensity ratio of D peak to G peak (I_D/I_G) were utilized to evaluate the graphitization degree of residual char, and lower I_D/I_G value indicated higher graphitization degree. [47-48] Here, the I_D/I_G value of ZIF-67@APP/EP was the lowest than them, indicating that the char residual of ZIF-67@APP/EP displayed the smallest microcrystal size and best char structure [49]. Therefore, the compact and continuous char layer may be the reasonable explanation for the satisfactory fire safety of ZIF-67@APP. [50]

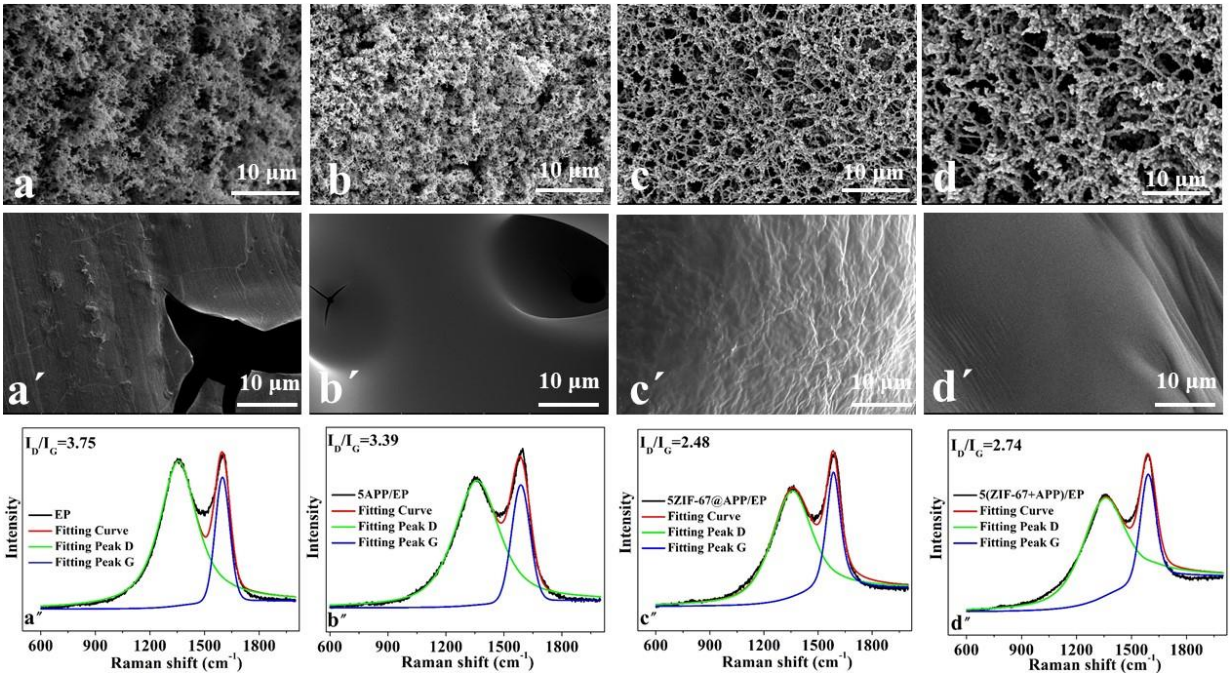

Figure 11. The exterior and interior SEM images and Raman spectra of char residual of pure EP (a, a´, a´´), 5APP/EP (b, b´, b´´), 5ZIF-67@APP/EP (c, c´, c ´´) and 5(ZIF-67+APP)/EP (d, d´, d´´) after CC test.

3.5 Flame-retardant mechanism of ZIF-67@APP/EPs

The results of CC and TG indicated that the char layer after burn-out of ZIF-67@APP could do better work on restraining the release of heat and smoke to reduce the fire hazard during burning. Thus, the formation process of char layer and flame-retardant mechanism of ZIF-67@APP on EP were investigated.

Firstly, the thermal decomposition process of APP, ZIF-67 and ZIF-67@APP were tested and the calculated curve of APP and ZIF-67 was also shown in Figure 12 and Figure S4. As seen in Figure 12, the thermal decomposition process of APP was divided into two steps, which showed the first step at 200-450 °C according to release the ammonia and H_2O during the thermal degradation of polyphosphate [7], and the second step was beyond 450 °C involving the elimination of phosphoric acid, polyphosphoric acid, and metaphosphoric acid with the decomposition of APP [51], respectively. For ZIF-67, only one decomposition process appeared at 517 °C. Whereas comparing with the calculated curve of APP and ZIF-67, the thermal decomposition started early and maximum weight loss rate of ZIF-67@APP at first decomposition step increased both N_2 and O_2 atmosphere. The phenomenon indicated that the ZIF-67 could accelerate the decomposition of APP and formation of the series structures of P-OH and Co^{2+}-APP [52-53]. When the temperature increased from 450 °C to 700 °C under N_2 atmosphere, the thermal decomposition step was divided into two steps and the maximum weight loss rate decreased obviously, and ZIF-67@APP displayed more residue up to 52.6 wt% from 27.9 wt% for APP at 700 °C, indicating that the synergistic effect existed between ZIF-67 and APP, which could promote the formation and the thermal stability of phosphorylation cross-linking structures at high temperature.

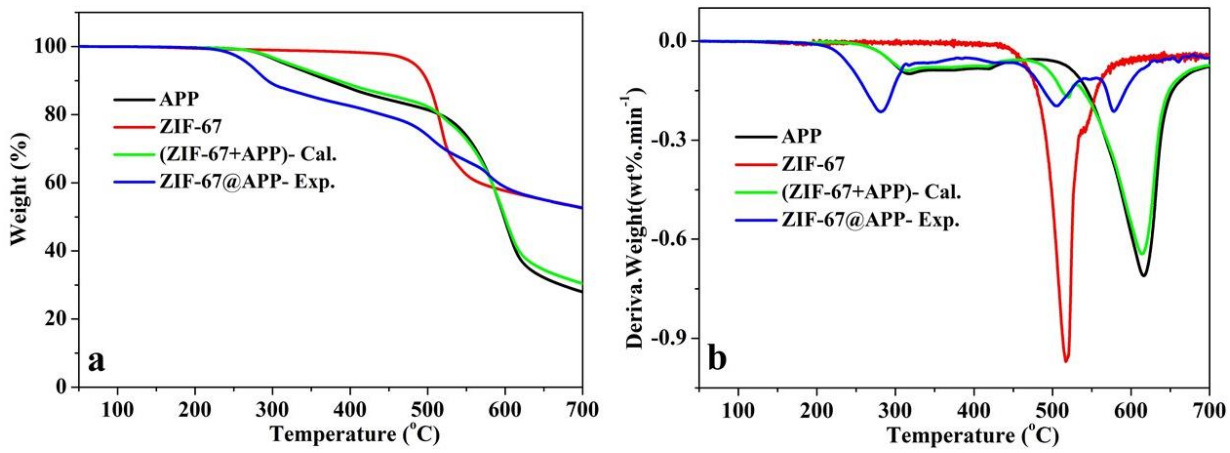

Figure 12. TG (a) and DTG (b) curves of APP, ZIF-67, (ZIF-67+APP)-calculated, and ZIF-67@APP-experimental under N_2 atmosphere.

The FTIR results for the condensed products of APP/EP and ZIF-67@APP/EP at different temperatures were displayed on Figure 13. Except other peaks, the peak at 1130.4 cm^{-1} was assigned to the structure of P-O-C [54]. As seen, the P-O-C in APP/EP started to appear at 450 °C and displayed a weak absorption. However, for ZIF-67@APP/EP, the P-O-C appeared at 400 °C, and the intensity increased with the temperature increase. In combination with the TG results, ZIF-67@APP could promote the formation of P-O-C, which could promote the thermal stability of residual.

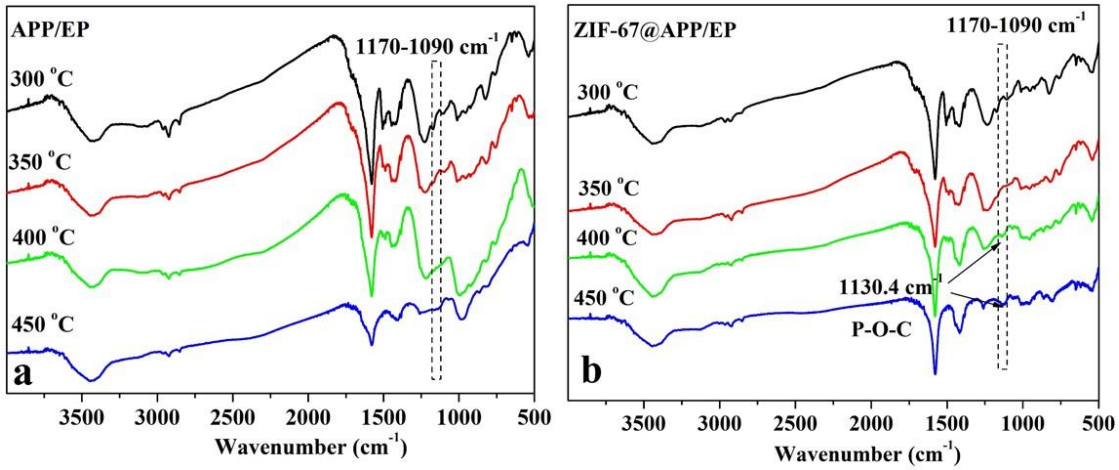

Figure 13. FTIR spectra for the condensed products of APP/EP (a) and ZIF-67@APP/EP (b) at different temperatures.

According to the TG results, all the EP materials had almost transformed into the char residual after 500 °C, however, these char residuals presented different behaviors in insulating the heat and smoke release. To further illustrate the difference of char residual among them as well as at different temperatures, the char structure was investigated by Thermo-Raman at 500 °C, 600 °C and 700 °C, and the results were exhibited in Figure 14. It could be observed that the I_D/I_G values of all samples tended to decrease when the temperature increased from 500 °C to 600 °C, while the I_D/I_G values increased with the temperature increase from 600 °C to 700 °C. It indicated that the char structures experienced a loose-compact-loose process with the temperature increasing. Nevertheless, I_D/I_G values at 700 °C were still lower than those at 500 °C. The results could also illustrate the stability of char layer on the high temperature. Interestingly, it was worthy noticed that ZIF-67@APP/EP all exhibited lowest I_D/I_G values than that of pure EP and APP/EP at 500 °C, 600 °C and 700 °C. Therefore, it could be concluded that the ZIF-67@APP could accelerate the generation of smallest microcrystal size of EP during combustion [55]. Meanwhile, the excellent char structure of ZIF-67@APP/EP could remain at high temperature, which could provide better protection the underlying EP from the transfer of heat and oxygen during combustion.

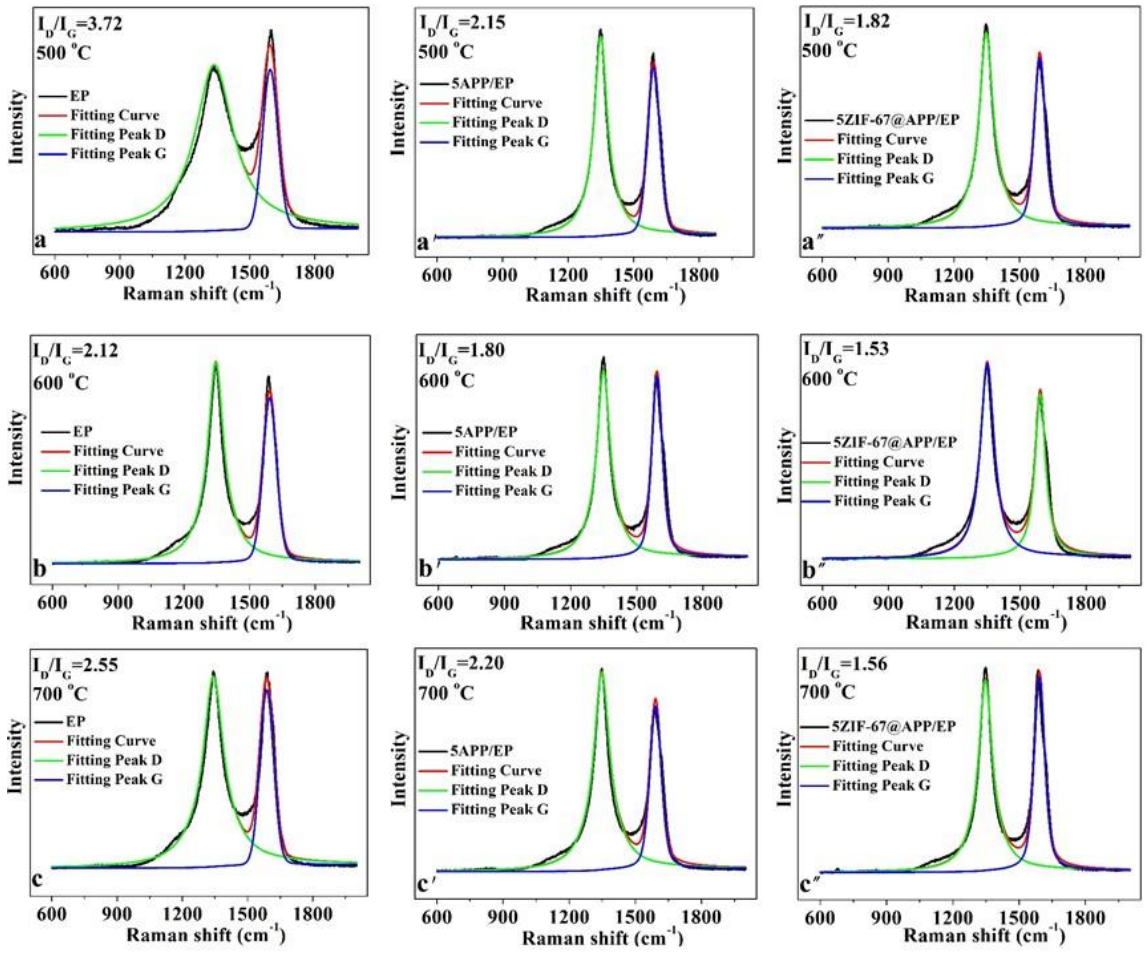

Figure 14. Thermo-Raman spectra of pure EP (a, b, c), 5APP/EP (a´, b´, c´), 5ZIF-67@APP/EP (a ´´, b´´, c ´´) at 500 °C, 600 °C and 700 °C

According to the Thermo-Raman, TG, and FTIR results, the flame-retardant mechanism can be concluded as follows. In the initial stage, Co^{2+} in ZIF-67@APP could accelerate the fast formation of the P-OH, then the structures of P-O-Co-O-C, P-O-C, etc. in the ZIF-67@APP/EP could form earlier than APP/EP, which could promote the fast formation of the char residue, so the fire safety could be obtained at the early combustion. With the temperature increase, more P-O-C and phosphorylation cross-linking structure structures generated and CoO_x appeared on the char layer accompanied by the release of H_2O and NH_3, and the compact and stable char

layer consisting of P-O-C, C=C, C-N, CoO_x, etc. was gradually formed at this stage, which could achieve excellent barrier during combustion process. Hence, the possible flame-retardant mechanism of ZIF-67@APP/EP during combustion process was shown in Figure 15.

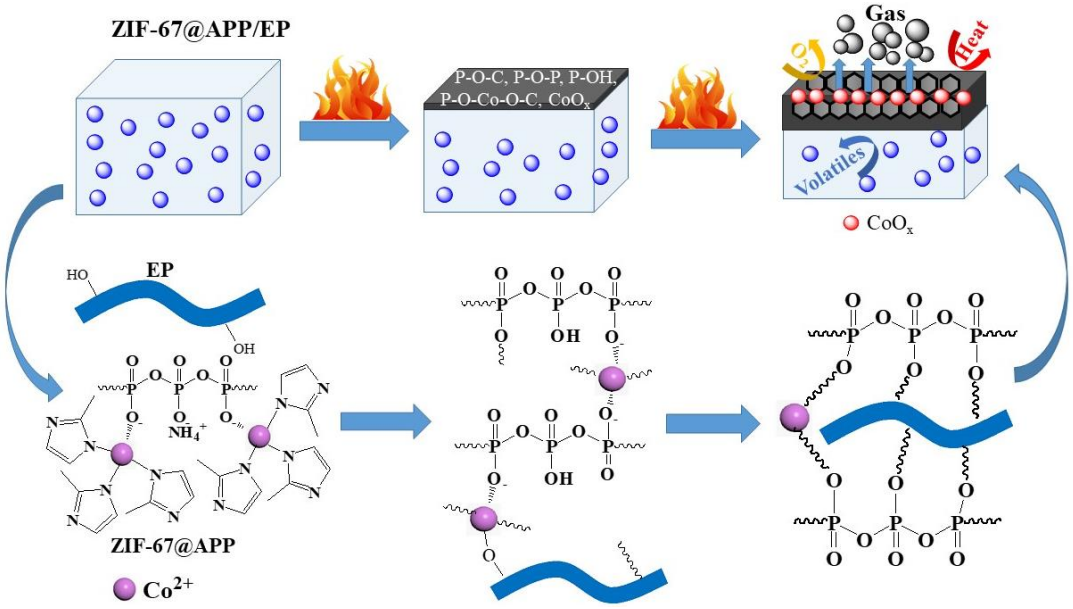

Figure 15. The possible flame-retardant mechanism of ZIF-67@APP/EP during combustion process.

4. Conclusions

In this work, a novel chemically modified method for APP (ZIF-67@APP) was designed and successfully obtained via interfacial assembly growth on the surface of APP. Owing to the better compatibility of ZIF-67@APP with EP, the mechanical properties of ZIF-67@APP/EP in terms of tensile and flexural strength were obviously improved compared to APP/EP. Besides, with the aid of the charring catalysis of ZIF-67@APP, ZIF-67@APP/EP could form a compact and stable intumescent char layer to insulate the transfer of oxygen and heat, and thus exhibited higher fire safety than APP/EP. On the basis of

the above, the anchoring of ZIF-67 on APP promises to offer a way to prepare excellent flame-retardant epoxy resins with satisfied mechanical properties.

Declaration of Competing Interest

The authors declare that they have no known competing financial interests or personal relationships that could have appeared to influence the work reported in this paper.

Acknowledgments

This work was partly supported by the National Natural Science Foundation of China (grant number 22075045 and 51673132), State Key Laboratory of Bio-Fibers and Eco-Textiles (Qingdao University, No. G2RC202013) and Open Foundation of Beijing Key Laboratory of Quality Evaluation Technology for Hygiene and Safety of Plastics (No. PQETGP2020004).

References

[1] Xu BR, Deng C, Li YM, Lu P, Zhao PP, Wang YZ. Novel amino glycerin decorated ammonium polyphosphate for the highly-efficient intumescent flame retardance of wood flour/polypropylene composite via simultaneous interfacial and bulk charring. Compos. Part B-Eng. 2019; 172: 636-648.

[2] Shao ZB, Deng C, Tan Y, Yu L, Chen MJ, Chen L, Wang YZ. Ammonium polyphosphate chemically-modified with ethanolamine as an efficient intumescent flame retardant for polypropylene. J. Mater. Chem. A 2014; 2: 13955-13965.

[3] Kim M, Ko H, Park SM. Synergistic effects of amine-modified ammonium polyphosphate on curing behaviors and flame retardation properties of epoxy composites. Compos. Part B-Eng. 2019; 170: 19-30.

[4] Xia SY, Zhang ZY, Leng Y, Li B, Xu MJ. Synthesis of a novel mono-component intumescent flame retardant and its high efficiency for flame retardant polyethylene. J. Anal. Appl. Pyrol. 2018; 134: 632-640.

[5] Wang JS, Wang DY, Liu Y, Ge XG, Wang YZ. Polyamide-enhanced flame retardancy of ammonium polyphosphate on epoxy resin. J. Appl. Polym. Sci. 2008; 108: 2644-2653.

[6] Khalili P, Tshai K, Hui D, Kong I. Synergistic of ammonium polyphosphate and alumina trihydrate as fire retardants for natural fiber reinforced epoxy composite. Compos. Part B-Eng. 2017; 114: 101-110.

[7] Yang HF, Guan YY, Ye L, Wang S, Li S, Wen X, Chen XC, Ewa M, Tang T. Synergistic effect of nanoscale carbon black and ammonium polyphosphate on improving thermal stability and flame retardancy of polypropylene: A reactive network for strengthening carbon layer. Compos. Part B-Eng. 2019; 174: 107038.

[8] Tan Y, Shao ZB, Yu LX, Long JW, Qi M, Chen L, Wang YZ. Piperazine-modified ammonium polyphosphate as monocomponent flame-retardant hardener for epoxy resin: flame retardance, curing behavior and mechanical property. Polym. Chem. 2016; 7: 3003-3012.

[9] Tan Y, Shao ZB, Chen XF, Long JW, Chen L, Wang YZ. Novel multifunctional organic–inorganic hybrid curing agent with high flame-retardant efficiency for epoxy resin. ACS Appl. Mater. Inter. 2015; 7: 17919-17928.

[10] Qiu SL, Ma C, Wang X, Zhou X, Feng XM, Yuen RKK, Hu Y. Melamine-containing polyphosphazene wrapped ammonium polyphosphate: A novel multifunctional organic-inorganic hybrid flame retardant. J. Hazard. Mater. 2018; 344: 839-848.

[11] Lewin M, Endo M. Catalysis of intumescent flame retardancy of polypropylene by metallic compounds. Polym. Adv. Technol. 2003; 14: 3-11.

[12] Davies PJ, Horrocks AR, Alderson A. The sensitisation of thermal decomposition of ammonium polyphosphate by selected metal ions and their potential for improved cotton fabric flame retardancy. Polym. Degrad. Stab. 2005; 88: 114-122.

[13] Zhang WW, Wu HJ, Meng WH, Li JH, Cui YM, Xu JZ, Qu HQ. Investigation of nickel ammonia phosphate with different morphologies as a new high-efficiency flame retardant for epoxy resin. High Perform. Polym. 2020; 32: 359-370.

[14] Chen MJ, Lin YC, Wang XN, Zhong L, Li QL, Liu ZG. Influence of cuprous oxide on enhancing the flame retardancy and smoke suppression of epoxy resins containing microencapsulated ammonium polyphosphate. Ind. Eng. Chem. Res. 2015; 54: 12705-12713.

[15] Zhang Y, Li XN, Fang ZP, Hull TR, Kelarakis A, Stec AA. Mechanism of enhancement of intumescent fire retardancy by metal acetates in polypropylene. Polym. Degrad. Stab. 2017; 136: 139-145.

[16] Zhang Y, Li XN, Cao ZH, Fang ZP, Hull TR, Stec AA. Synthesis of zinc phosphonated poly(ethylene imine) and its fire-retardant effect in low density polyethylene. Ind. Eng. Chem. Res. 2015; 54: 3247-3256.

[17] Khalili P, Liu XL, Tshai KY, Rudd C, Yi XS, Kong I. Development of fire retardancy of natural fiber composite encouraged by a synergy between zinc borate and ammonium polyphosphate. Compos. Part B-Eng. 2019; 159: 165-172.

[18] Cao ZH, Zhang Y, Song PA, Cai YZ, Guo Q, Fang ZP, Peng M. A novel zinc chelate complex containing both phosphorus and nitrogen for improving the flame retardancy of low density polyethylene. J. Anal. Appl. Pyrolysis 2011; 92: 339-346.

[19] Hou YB, Qiu SL, Hu Y, Kundu CK, Gui Z, Hu WZ. Construction of bimetallic ZIFs derived Co-Ni LDHs on the surfaces of GO or CNTs with a recyclable method: towards reduce toxicity of gaseous thermal decomposition products of unsaturated polyester resin, ACS Appl. Mater. Interfaces 2018;10: 18359-18371.

[20] Yang S, Lin X, Lewis W, Suyetin M, Bichoutskaia E, Parker JE, Tang CC, Allan DR, Rizkallah PJ, Hubberstey P. A partially interpenetrated metal–organic framework for selective hysteretic sorption of carbon dioxide. Nat. Mater. 2012; 11: 710-716.

[21] Wang L, Han YZ, Feng X, Zhou JW, Qi PF, Wang B. Metal-organic frameworks for energy storage: batteries and supercapacitors. Coord. Chem. Rev. 2016; 307: 361-381.

[22] Zhang RR, Hu L, Bao SX, Li R, Gao L, Li R, Chen QW. Surface polarization enhancement: high catalytic performance of Cu/CuOx/C nanocomposites derived from Cu-BTC for CO oxidation. J. Mater. Chem. A 2016; 4: 8412-8420.

[23] Zhang YF, Pan AQ, Ding L, Zhou ZL, Wang YP, Niu SY, Liang SQ, Cao GZ. Nitrogen-doped Yolk–shell-structured CoSe/C Dodecahedra for High-performance Sodium Ion Batteries. ACS Appl. Mater. Inter. 2017; 9: 3624-3633.

[24] Liu C, Mullins M, Hawkins S, Kotaki M, Sue HJ. Epoxy nanocomposites containing zeolitic imidazolate framework-8. ACS Appl. Mater. Inter. 2018; 10: 1250-1257.

[25] Hou YB, Hu WZ, Gui Z, Hu Y. Preparation of metal-organic frameworks and their application as flame retardants for polystyrene. Ind. Eng. Chem. Res. 2017; 56: 2036-2045.

[26] Guo WW, Nie SB, Kalali EN, Wang X, Wang W, Cai W, Song L, Hu Y. Construction of SiO2@UiO-66 core–shell microarchitectures through covalent linkage as flame retardant and smoke suppressant for epoxy resins. Compos. Part B-Eng. 2019; 176: 107261.

[27] Shi XW, Dai X, Cao Y, Li JW, Huo CG, Wang XL. Degradable poly(lactic acid)/metal-organic framework nanocomposites exhibiting good mechanical, flame retardant, and dielectric properties for the fabrication of disposable electronics. Ind. Eng. Chem. Res. 2017; 56: 3887-3894.

[28] Qi XL, Zhou D, Zhang J, Hu S, Haranczyk M, Wang DY. Simultaneous improvement of mechanical and fire-safety properties of polymer composites with phosphonate-loaded MOF additives. ACS Appl. Mater. Inter. 2019; 11: 20325-20332.

[29] Lv XY, Zeng W, Yang ZW, Yang YX, Wang Y, Lei ZQ, Liu JL, Chen DL. Fabrication of ZIF-8@Polyphosphazene core-shell structure and its efficient synergism with ammonium polyphosphate in flame-retarding epoxy resin. Polym. Adv. Technol. 2020; 31: 997-1006.

[30] Zhang J, Li Z, Zhang L, Molleja JG, Wang DY. Bimetallic metal-organic frameworks and graphene oxide nano-hybrids for enhanced fire retardant epoxy composites: A novel carbonization mechanism. Carbon 2019; 153: 407-416.

[31] Wang JY, Shi H, Zhu PL, Wei YJ, Hao JW. Ammonium polyphosphate with high specific surface area by assembling zeolite imidazole framework in eva resin: significant mechanical properties, migration resistance, and flame retardancy. Polymers 2020; 12: 534.

[32] Du XD, Wang CC, Liu JG, Zhao XD, Zhong J, Li YX, Li J, Wang P. Extensive and selective adsorption of ZIF-67 towards organic dyes: Performance and mechanism. J. Colloid Interface Sci. 2017; 506: 437-441.

[33] Qian JF, Sun F, Qin LZ. Hydrothermal synthesis of zeolitic imidazolate framework-67 (ZIF-67) nanocrystals. Mater. Lett. 2012; 82: 220-223.

[34] Bourbigot S, Bras ML, Gengembre L, Delobel R. XPS study of an intumescent coating application to the ammonium polyphosphate/pentaerythritol fire-retardant system. Appl. Surf. Sci. 1994; 81: 299-307.

[35] Bourbigot S, Bras ML, Delobel R. Carbonization mechanisms resulting from intumescence association with the ammonium polyphosphate-pentaerythritol fire retardant system. Carbon 1993; 8: 1219-1230.

[36] Huo SQ, Yang S, Wang J, Cheng JW, Zhang QQ, Hu YF, Ding GP, Zhang QX, Song PA. A liquid phosphorus-containing imidazole derivative as flame-retardant curing agent for epoxy resin with enhanced thermal latency, mechanical, and flame-retardant performances. J. Hazard Mater. 2020; 386: 121984.

[37] Jian RK, Lin XB, Liu ZQ, Zhang W, Zhang J, Zhang L, Li Z, Wang DY. Rationally designed zinc borate@ZIF-8 core-shell nanorods for curing epoxy resins along with low flammability and high mechanical property. Compos. Part B-Eng. 2020; 200: 108349.

[38] Xu YJ, Chen L, Rao WH, Qi M, Guo DM, Liao W, Wang YZ. Latent curing epoxy system with excellent thermal stability, flame retardance and dielectric property. Chem. Eng. J. 2018; 347: 223-232.

[39] Zhang FQ, Wang B, Xu YJ, Li P, Liu Y, Zhu P. Convenient blending of alginate fibers with polyamide fibers for flame-retardant non-woven fabrics. Cellulose 2020; 27: 8341-8349.

[40] Ai YF, Pang FQ, Xu YL, Jian RK. Multifunctional Phosphorus-containing triazolyl amine toward self-intumescent flame-retardant and mechanically strong epoxy resin with high transparency. Ind. Eng. Chem. Res. 2020; 59: 11918-11929.

[41] Zhao B, Liu PW, Liu DY, Kolibaba TJ, Zhang CY, Liu YT, Liu YQ. Functionalized graphene oxide based on hydrogen-bonding interaction in water: preparation and flame-retardation on epoxy Resin. Macromol. Mater. Eng. 2019; 304: 1900164.

[42] Breulet H, Steenhuizen T. Fire testing of cables: comparison of SBI with FIPEC/Europacable test. Polym. Degrad. Stab. 2005; 88: 150-158.

[43] Zhao HB, Chen MJ, Chen HB. Thermally insulating and flame-retardant polyaniline/pectin aerogels. ACS Sustain. Chem. Eng. 2017; 5: 7012-7019.

[44] Dong CH, Ling S, Ma XB, Zhou L, He PS, Zhu P. Synthesis of a novel linear α, ω-Di (chloro phosphoramide) polydimethylsiloxane and its applications in improving flame-retardant and water-repellent properties of cotton fabrics. Polymers 2019; 11: 1829.

[45] Li P, Wang B, Liu YY, Xu YJ, Jiang ZM, Dong CH, Zhang L, Liu Y, Zhu P. Fully bio-based coating from chitosan and phytate for fire-safety and antibacterial cotton fabrics. Carbohyd. Polym. 2020; 237: 116173.

[46] Wen X, Liu ZQ, Li Z, Zhang J, Wang DY, Szymanska K, Chen XC, Mijowska E, Tang T. Constructing multifunctional nanofiller with reactive interface in PLA/CB-g-DOPO composites for simultaneously improving flame retardancy, electrical conductivity and mechanical properties. Compos. Sci. Technol. 2020; 188: 107988.

[47] Wang RY, Lu GM, Qiao WM, Yu JG. Catalytic Graphitization of Coal-Based Carbon Materials with Light Rare Earth Elements. Langmuir 2016; 32: 8583-8592.

[48] Xu YJ, Qu LY, Liu Y, Zhu P. An overview of alginates as flame-retardant materials: Pyrolysis behaviors, flame retardancy, and applications. Carbohyd. Polym. 2021; 260: 117827.

[49] Li Z, Zhang JH, Dufosse F, Wang DY. Ultrafine nickel nanocatalyst-engineering organic layered double hydroxide towards super-efficiently fire-safe epoxy resin via interfacial catalysis. J. Mater. Chem. A 2018; 6: 8488-8498.

[50] Wang B, Li P, Xu YJ, Jiang ZM, Dong CH, Liu Y, Zhu P. Bio-based, nontoxic and flame-retardant cotton/alginate blended fibres as filling materials: thermal degradation properties, flammability and flame-retardant mechanism. Compos. Part B-Eng. 2020; 194: 108038.

[51] Liu GS, Chen WY, Yu JG. A novel process to prepare ammonium polyphosphate with crystalline form ii and its comparison with melamine polyphosphate. Ind. Eng. Chem. Res. 2010; 49: 12148-12155.

[52] Li WX, Liao DJ, Hu XP, Cheng Z, Xie CQ. Synergistic improvement of fire retardancy and mechanical properties of ferrocene-based polymer in intumescent polypropylene composite. Polym. Adv. Technol. 2019; 30: 2402-2413.

[53] Li WX, Zhang HJ, Hu XP, Yang WX, Cheng Z, Xie CQ. Highly efficient replacement of traditional intumescent flame retardants in polypropylene by manganese ions doped melamine phytate nanosheets. J. Hazard. Mater. 2020; 398: 123001.

[54] Wang X, Zhou S, Xing WY, Yu B, Feng XM, Song L, Hu Y. Self-assembly of Ni–Fe layered double hydroxide/ graphene hybrids for reducing fire hazard in epoxy composites. J. Mater. Chem. A 2013; 1: 4383-4390.

[55] Zhang AN, Zhao HB, Cheng JB, Li ME, Li SL, Cao M, Wang YZ. Construction of durable eco-friendly biomass-based flame-retardant coating for cotton fabrics. Chem. Eng. J. 2021; 410: 128361.